ISSN 1392–1320 MATERIALS SCIENCE (MEDŽIAGOTYRA). Vol. XX, No. X. 2023

Investigating the Effect of Fe_2O_3 on Wear Behaviour and Corrosion Resistance of Electroless Ni–P Coating with Different Fe_2O_3 Concentrations on AISI 4140 Steel

Ahlam Hamid JASIM [1] *, Abdul Raheem Kadim ABIDALI [2], Alaa Mohammed Hussein WAIS [3]

[1] *Al-Qasim Green University, College of Engineering, Hillah, Babil, Iraq*
[2] *University of Babylon, College of Material Engineering 51001 Hillah, Babil, Iraq*
[3] *Biomedical Engineering Department, Al-Mustaqbal University College, 51001 Hillah, Babil, Iraq*

crossref http://dx.doi.org/10.5755/j02.ms.31937

Received 09 August 2022; accepted 04 October 2022

In this study, Ni–P–Fe_2O_3 composite was deposited on AISI 4140 steel using different concentrations of Fe_2O_3 ranging from 0.1 to 0.5 gr/lit in an electroless bath. The phase analysis and surface morphology of the samples were characterized using X-ray diffraction and FESEM. The corrosion behavior of the coated samples was investigated in a 3.5 wt. % NaCl solution through potentiodynamic polarization. The results of the potentiodynamic test show that adding Fe_2O_3 into an electroless bath facilitates the formation of the passive layer. The results show that the coating created at a thickness of (10-16µm) had the highest corrosion resistance compared to other coated and non-coated samples. Furthermore, the results of the friction coefficients of the samples produced by powder metallurgy have decreased because Fe_2O_3 particles led to a decrease in grain size in the heat treatment of specimens and prevented excessive heat generation during the wear test; thus, the friction coefficient decreased during the test.
Keywords: electroless Ni-P–Fe_2O_3 coating, heat treatment, microhardness, wear resistance and resistance of corrosion.

1. INTRODUCTION

AISI 316L SS is a common implant material because of its reasonable cost, easy accessibility, excellent manufacturing properties, accepted biocompatibility, and good performance in corrosion resistance, making this material extremely attractive in the application of implant materials [1]. An electroless nickel coating enhances wear, friction, and corrosion resistance, increases the material's surface hardness, creates a thick and homogeneous coating, and, in many circumstances, retains the material's original surface finish. Additionally, it possesses excellent electrical and thermal conductivity, lubricity, and ductility [2].

Steel, aluminum, and copper alloys may all have a chemical nickel coating to make them more durable and brighter. Its high mechanical qualities make steel the most used substrate material. In terms of economics, steel and aluminum are competing. In the electroless Ni–P coating structure, the phosphorus component causes the coating to be an amorphous deposit. After increasing temperature, the amorphous structure breaks down into a crystallized one. There is a considerable increase in hardness and wear resistance after heat treatment [4]. To better lubricate and protect the plated surface from corrosion, some composite coatings incorporate particles like graphite PTFE and MoS_2, while others use more rigid particles like Si_3N_4, WC, Al_2O_3, TiO_2, and SiC [5, 6]. These hard particles are used in the latter type of composite coating to increase hardness, wear resistance (friction and wear), and corrosion resistance (corrosion). The electroless nickel plating technique is widely used in many fields and allows a high-performance product with high hardness, wear resistance, and corrosion resistance. There are several advantages of this method, such as; low cost and easy formation of a continuous and uniform coating on the surface of the substrate with a complex shape [27]. SEM electron microscopy was used to examine the microstructure of electroless nickel coatings, providing vital information on the phase change during heat treatment. When heated to 400 °C for one-hour, various nickel phosphide Ni3P particles precipitated.

Consequently, EN coatings underwent significant alterations in many characteristics [7]. For photo-electrochemical cells for hydrogen production, metal oxide semiconductors such as TiO_2, Fe_2O_3, WO_3, etc., have been studied [8]. Metal ion dopants may affect the recombination rates of electron-hole pairs [8]. Electricity-free nickel used to be widely employed in many sectors, including the car and aeronautics industry(s), but it has since been phased out in favor of more environmentally friendly processes [9].

The aim of the present study is to understand the effect of Fe_2O_3 concentration on the corrosion behavior of the electroless Ni–P–Fe_2O_3 coating. To do so, the corrosion behavior of the specimens was assessed by potentiodynamic polarization technique and the mechanical properties (microhardness and wear) of the 4140 steel.

2. EXPERIMENTAL

2.1. Substrate preparation

The substrate metal used in this study was 4140 steel. Samples of 20 mm × 10 mm (diameter × height) were used as the base metal.

* Corresponding author. Tel.: +9647806039856.
E-mail address: *ahlam.hamid@wrec.uoqasim.edu.iq* (A.H. Jasim)

Table 1. Chemical Compositions of 4140 steel

Element	C	Si	S	Mn	P	Cr	Mo	Fe
AISI	0.3 – 0.45	max 0.4	max 0.003	0.6 – 0.9	max 0.03	0.9 – 1.2	0.15 – 0.3	Bal.
wt.%	0.40	0.29	0.01	0.67	0.01	0.95	0.2	Bal.

The chemical analysis for this alloy and the composition details (wt.%) are shown in Table 1. Emery paper (tungsten oxide paper) No. 180 – 2000 was used to grind and polish all specimens, wash them in distilled water and ethanol and then dry them. For 30 min, they were submerged in acetone and polished using diamond paste. At 60 °C and 30 g/L NaOH, $NaCO_3$, and $NaPbO_4$, specimens were soaked for one minute in the solution before being coated. Magnetic stirring with a 5-volt power source was used to remove any oil and particles from the metal surface of the electrolyte. After that, the samples were washed in distilled water and dried using an electric dryer before being immersed in the coating solution. Finally, the samples were dried using an electric dryer, and the specimens were placed in glass storage containing particles of silica gel to absorb any wetness and protect the samples from corrosion.

2.2. Electroless bath preparation

After the surfaces had been prepared for coating, an electroless bath was prepared, according to concentrations shown in Table 2.

Table 2. Operating conditions for an electroless bath

Bath composition	g/L
Nickel chloride ($NiCl_2{\cdot}6H_2O$)	30
Sodium hypophosphite (NaH_2Po_2)	10
Amina chloride	50
Sodium citrate	84
Fe_2O_3	0.1, 0.3, 0.5
Operating conditions	
PH	6 – 8
Temperature	95 °C
Time	1 HR

The NiP plating was deposited on the substrate during the process of coating. The pH value for the coating bath was between 6 and 8. The electroless Ni–P coating was conducted at 95 ± 1 °C for 60 min. The bath solution was mixed using a magnetic stirrer with a decrease in the fluctuations of ionic concentrations through plating. The sample was mixed in a two-way direction every 10 min to produce a uniformly thick coating. The Ni–P–Fe_2O_3 coating deposition had different concentrations of Fe_2O_3 (0.1 g/L, 0.3 g/L and 0.5 g/L). Fig. 1 shows the experimental setup for the electroless deposition process. After the coating process was completed, specimens were placed inside a vacuum oven at 50 °C to dry for 30 min.

2.3. Nano iron oxide preparation

Iron oxide nanopowder was prepared using a chemical precipitation route. Hydrated ferric chloride ($FeCl_3{\cdot}6H_2O$) was dissolved in 50 % ethyl alcohol with 0.5M at 45 °C using 1000 rpm as the rotation of the magnetic stirrer. Glucose with a 7 % concentration solution was added to the solution at 5 ml/l, which acts as surfactant material to avoid growth.

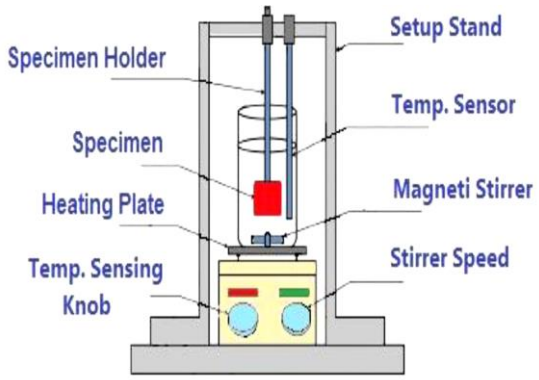

Fig.1. Experimental setup for the electroless deposition process

Dropwise, ammonium hydroxide was added to the solution to obtain a thick gel. Furthermore, filtration and washing with deionized water were done, drying at 100 °C for six-hour and calcined at 400 °C for one hour. The obtained powder was crushed in alumina mortar and examined with high-resolution transmission electron microscopy to reveal particle size and distribution.

2.4. Heat treatment of coated samples

After the deposition, the annealing process was conducted for all samples (Ni–P and Ni–P–Fe_2O_3) in a vacuum furnace at 400 °C for one hour. With a digital coating of thickness gage type (TT260 country), which is used to determine coating thickness, the thickness range coating is determined (10 – 16 µm) on the substrate surface.

2.5. Characterization

The initial microstructure of the low alloy steel 4140 was examined using optical microscopy. The size and distribution of particles may be determined using high-resolution transmission electron microscopy (TEM, JOEL 1210l). Surface morphologies and compositions of the Ni–P–Fe_2O_3 composite coatings were examined using scanning electron microscopy with an energy dispersive X-ray spectroscopy (SEM/EDX, JOEL JSM-6390 LVSEM). It was determined that the coatings have crystalline phases. The crystal structure of the specimens was detected using EQuinox (3000) (XRD) and Cu Ka (X = 1.54187 Å) radiation at roughly 40 kV and 30 mA. A standard parameter, R_a in µ, was used to compute the surface roughness measurement value of the coated samples before and after heat treatment. Measurements of R_a were made using a surface roughness tester called the HER210 model, which has an accuracy of 0.05 µm. A TH-717 Vickers hardness tester was used to assess the microhardness of the coating layers after a force of 25 g was applied for 15 s. Each coated specimen received three measurements, with the substrate receiving a fourth. The average value was then calculated. Pin-on-disc wear testing was used to evaluate (ASTM G 99 standard). The weight of the load employed was 10 N. It was 376 meters of sliding at a pace of 0.1 m/s.

Carbonized steel made up the disc. Before and after the wear test, the specimens were weighed on a precise scale to determine how much plating was lost. Assuming a sliding distance of l and an average load of L, the specific wear rate $Ws = w/(l \cdot L)$ was determined. It could predict the coatings' corrosion behaviour with the Tafel extrapolation approach. Therefore, measuring the corrosion potential and voltage difference between a metal submerged in a specific environment and the corrosion current density (I_{corr}) in a 3.5 % NaCl solution and the corrosion rate coatings.

3. RESULTS AND DISCUSSION

3.1. Optical microscope

The initial microstructure of the low alloy steel 4140, which is the base metal of the composition, has been listed in Table 1. The microstructures of 4140 steel were noted after being etched for 10 min in a 5 ml HCl solution and 100 ml 95 % ethanol solution (E ASTM 407-99). The microstructure of this alloy is shown in Fig. 2.

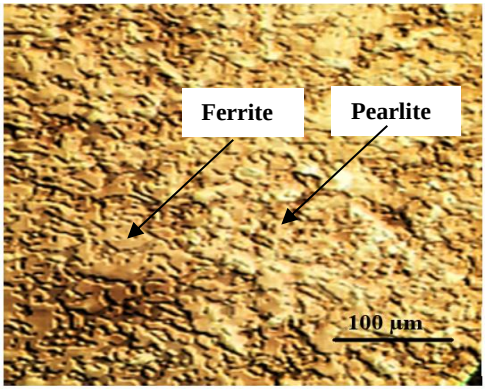

a

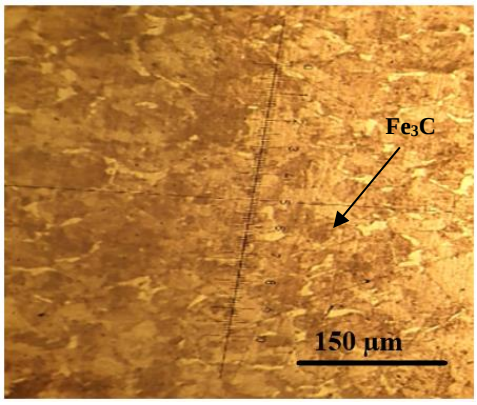

b

Fig. 2. Microstructure from the centre of 4140 steel before coating: a – 400x magnification; b – 600x magnification

Pearlite is made up of ferrite interwoven with cementite laths (Fe_3C). The microstructure revealed ferrite and pearlite-rich regions at low magnification (400^x). As demonstrated in Fig. 2 b, the pearlite was interwoven in the pearlite-rich bands. Furthermore, the microstructure shows isolated pearlite that is smaller than linked pearlite. Isolated pearlite colonies were mainly found at triple points or grain borders. The grain morphology of the ferrite was uneven, with a grain size of roughly 10 µm. As seen in Fig. 2, most ferrite grain boundaries were bent. This is a ferrite microstructure matching carbon steel with less than 0.6 % carbon, which is the case of the carbon steel examined in this paper. The cementite phase in carbon steel is hard and brittle, and it may be the most prone to corrosion, particularly in isolated forms.

3.2. Transmission electron microscopy

The TEM images of Nano iron oxide particle size and distribution are shown in Fig. 3. The analysis of EDX local in Fig. 4 explains the presence of nano iron oxide particles.

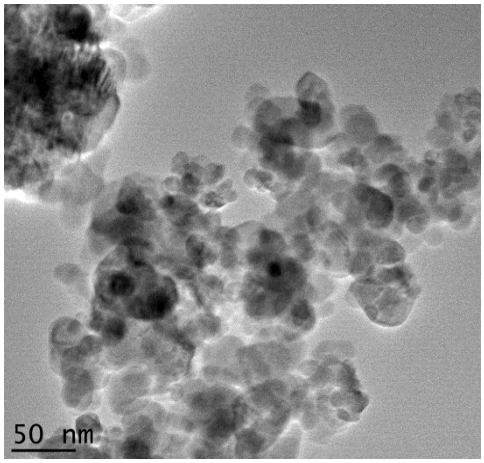

a

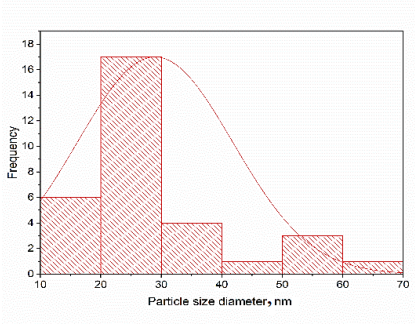

b

Fig. 3. TEM of nano iron oxide particle size and its distribution

Fig. 3 a shows that most particles were almost spherical, with potentially excellent dispersity and negligible agglomeration. The occurrence of agglomeration might be owing to van der Waals forces that bind particles together and shear forces that can be applied at the nanoscale. Furthermore, the presence of hydroxyl groups in the peel extract may have contributed to agglomeration. Fig. 3 b depicts a histogram of the NP size distribution with 32 counts. The size ranged from 10 to 61 nm, with a mean size of 28.965 nm and a standard deviation of 1.448 nm. Fig. 4 shows the energy-dispersive X-ray spectra (EDX). The presence of carbon, oxygen and iron in produced nanoparticles is shown by EDX spectrum analysis.

3.3. Surface morphology

The SEM images of the Ni–P–Fe_2O_3 composite coating are shown in Fig. 5. The composite electroless coating deposited from the coating bath containing 0.1 g/L Fe_2O_3 particles that distributed spherical-like growths on the deposition surface can be noted in Fig. 5.

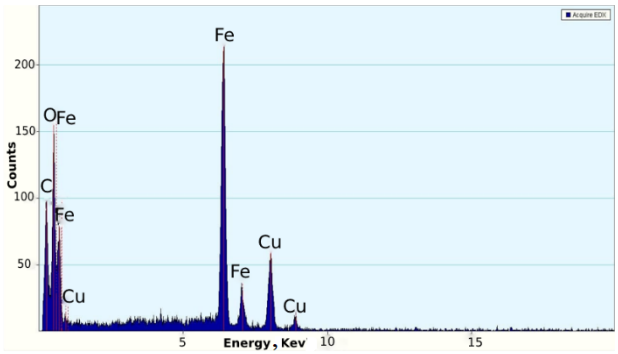

Fig. 4. Analysis of EDX for nano iron oxide particles

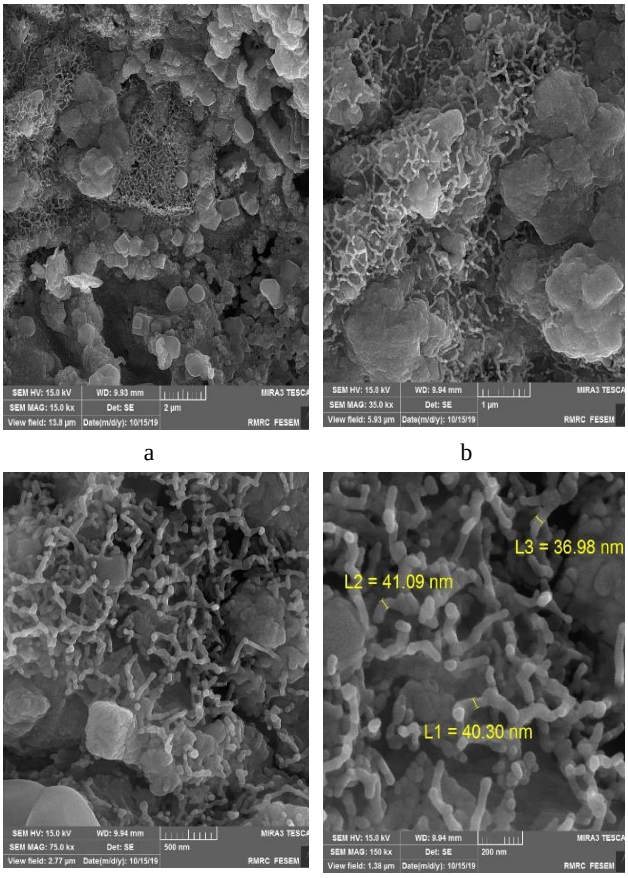

a b c d

Fig. 5. FESEM of coated electroless of Ni–P–0.1g/l Fe_2O_3 and annealed: a – 2 µm; b – 1 µm; c – 500 nm; d – 200 nm magnification

It is indicated that Fe_2O_3 particles were inside the Ni–P deposits, especially embedded into the spherical-like structures. The analysis of EDX in Fig. 6 explains the presence of Fe_2O_3 particles. The investigations discovered that Fe_2O_3 particles do not limit the Ni^{2+} deposition while it deposits at the top [10].

3.4. XRD characterization

XRD patterns of the Ni–P–Fe_2O_3 (0.1 g/L Fe_2O_3) sample as-annealed at 400 °C for 1 h are presented in Fig. 6. The addition of Fe_2O_3 in the matrix of Ni–P led to the crystalline nature of the Ni–P–Fe_2O_3 alloy, which can be attributed to the lower phosphorous content than in the binary Ni–P. When the procedure of heat treatment (400 °C for 1 h) for Ni–P–Fe_2O_3 coating was clear, peaks of the Ni3P phase were prominent along with recrystallization of Ni [9 – 11].

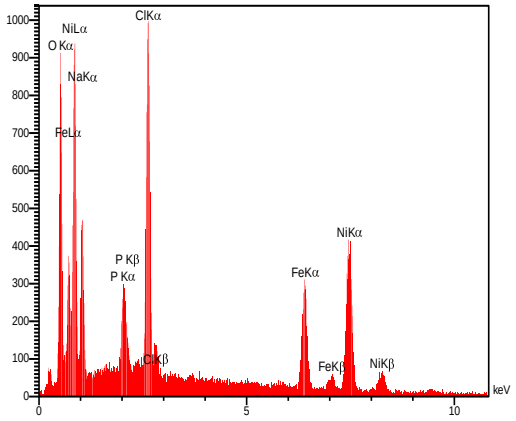

Fig. 6. Analysis of EDX for the surface of Ni–P–Fe_2O_3 coating

The presence of Ni and Ni3P phases in the coating was observed in Fig. 7. The crystalline phase of Ni and Ni3P were the predominant phases induced by the heat treatment of the coating. The formation of these phases by heat treatment of Ni–P–Fe_2O_3 (0.1 g/L Fe_2O_3) electroless coatings was also shown by other researchers [11].

3.5. Surface roughness

Data regarding the roughness of the base metal of plated and annealed specimens has been illustrated in Table 3. There is a noticeable difference in the Ni–P electrode's surface roughness value (0.12) compared to that of the Fe_2O_3 mixed oxide-incorporated Ni-P electrode (0.16 – 0.24). This demonstrates that the surface roughness change happened during the mixed oxide's assimilation. In order to obtain the roughness factor R_f, the double layer capacitance of the coatings C_{dl} was divided by the smooth electrode's 20 µF capacitance.

$$R_f = \frac{C_{dl}}{20\mu F}. \quad (1)$$

As mentioned above, an increase in Fe_2O_3 concentration at 0.5 g/L causes a significant increase in roughness. Fe_2O_3 prevents the constant growth of Ni and creates roughness. The sample roughness of Ni–P–Fe_2O_3 (0.5 g/L Fe_2O_3) is higher when compared with other specimens, as a large concentration of Fe_2O_3 may result in agglomeration, which was also shown by other researchers [11].

Table 3. Result of samples surface roughness

Specimen	R_a, µ
Substrate (4140)	0.28 ± 0.014
Ni–P plated	0.12 ± 0.006
Ni–P–0.1 g/L Fe_2O_3 plated	0.16 ± 0.008
Ni–P–0.3 g/L Fe_2O_3 plated	0.2 ± 0.01
Ni–P–0.5 g/L Fe_2O_3 plated	0.24 ± 0.012
Ni–P annealed	0.25 ± 0.0125
Ni–P–0.1 g/L Fe_2O_3 annealed	0.2 ± 0.01
Ni–P–0.3 g/L Fe_2O_3 annealed	0.24 ± 0.012
Ni–P–0.5 g/L Fe_2O_3 annealed	0.3 ± 0.015

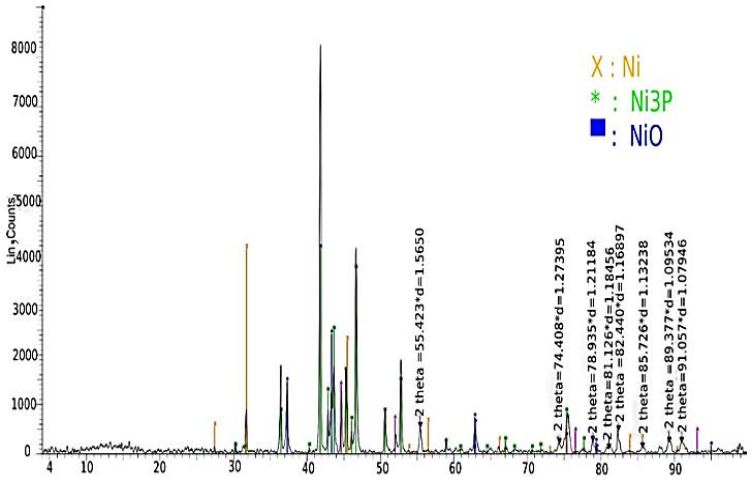

Fig. 7. X-ray diffraction patterns of annealed Ni–P–0.1 g/L Fe_2O_3 sample

3.6. Microhardness

Fig. 8 shows the surface microhardness of the samples that underwent heat treatment. Fe_2O_3 can enhance the microhardness of a surface, particularly in the sample of Ni–P–Fe_2O_3 (0.1 g/L Fe_2O_3). These results can be associated with the reinforcement and uniform distribution of Fe_2O_3 in these specimens due to the positive charge during deposition of the bath dispersions with a pH of ~6. The incorporating Fe_2O_3 particles had higher hardness [12, 13] than Ni–P and also had a dispersion-strengthening effect in the composite matrix and produced grain refining [14 – 16]. All these parameters contributed toward the general enhancement of the microhardness of the composite coating. The hardness of Ni–P–Fe_2O_3 (0.5 g/L Fe_2O_3) is less when compared with the specimen containing 0.1 g/L Fe_2O_3, owing to the large concentration of Fe_2O_3; in addition to this, lousy cohesion with the matrix Ni–P at the composite led to a decrease in the microhardness of the coated layer [17]. The increase in microhardness by heat treatment can be related to transforming the amorphous structure into a crystalline one [18]. A Yönetken [25] indicated that Ni plating of powders results in higher hardness values. The protruding tip of the hardness tester generates a limited deformation because of the readily deformable Ni layer existing on the particles and therefore results in higher hardness readings in Ni plated specimens, whereas the protruding tip of the hardness tester causes a complete deformation and breaks apart the particles in non-plated specimens, lowering the hardness readings

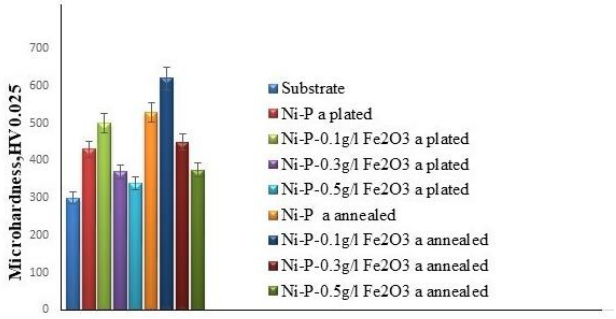

Fig. 8. Microhardness of plated and annealed specimen's surface

3.7. Wear behaviour

Wear, and friction tests were performed on composite coatings comprising varying amounts of embedded Ni–P–Fe_2O_3 particles under identical testing machine settings. The width of the wear tracks, measured under the circumstances indicated, was used to determine the degree of wear induced at sliding contact sites. As shown in Fig. 8, typical wear tracks were microscopically captured under the previously stated circumstances. The micrographs demonstrated that the composite coating's wear track was thinner than the pure nickel coating's. Pure and composite coatings had different wear track widths, indicating different resistance to wear propagation owing to matrix hardening caused by Fe_2O_3 particle embedding, whereas Fe_2O_3 particles did not harden the nickel matrix.

Fig. 9 indicates the relationship between the friction coefficient and distance for the annealed samples; it can be noted in sample Ni–P.

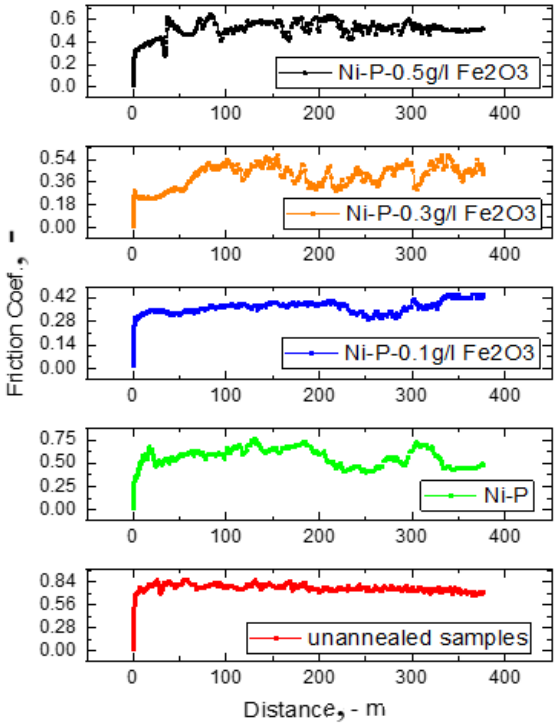

Fig. 9. The friction coefficient differences as a function of distance

Due to the high solubility of nickel and iron, this consequence may lead to a higher amount of material removal from the surface and an increase in surface contact with the counterpart. During the wear test, the crystallization of an amorphous, plated specimen may also factor in this behaviour. When Fe_2O_3 concentrations rise over 0.1 %, friction diminishes. This might be attributed to the easy shear and rolling of the lubricating film contained particles, which reduces direct contact between sample counterparts on the surface [10].

Table 4 explains the specific wear rate and heat-treated samples' average friction coefficient. The friction coefficient obtained in this study was between 0.42 and 0.68 according to the chemical composition of the substrate material is also compatible with the literature [24]. It noted a decrease in the wear rate of the substrate with applying (Ni–P) and (Ni–P–Fe_2O_3) composite coating, respectively. As noted, the friction coefficient is related to the specific wear rate. In this behavior, composite coatings improve the substrate wear resistance because of an increase in microhardness due to the addition of Fe_2O particles in the composite coatings. An annealed Ni–P–Fe_2O_3 (0.1 g/l Fe_2O_3) had a lower specific wear rate than the other specimens because it had the lowest coefficient of friction and larger microhardness, more acceptable grain size, and a homogenous distribution of Ni3P and Ni particles.

Increasing microhardness caused a decrease in the wear rate and the formation of phases after the treatments. It also caused the low mutual solubility between those phases. Iron may be used to increase wear resistance [18]. A Yönetken [26] The rise in the hardness and strength values is encouraging for a low wear volume with relatively high hardness composite materials having a limited ductile property.

Table 4. Friction coefficient and specific wear rate of an annealed coating specimen

Sample	Coefficient of friction	Specific wear rate, $mm^3/N{\cdot}m{\cdot}10^{-4}$
Substrate	0.68 ± 0.034	1.3 ± 0.065
Ni–P annealed	0.49 ± 0.024	0.4 ± 0.02
Ni–P–0.1 g/L Fe_2O_3 annealed	0.42 ± 0.021	0.13 ± 0.006
Ni–Co–P–0.3 g/L Fe_2O_3 annealed	0.46 ± 0.023	2.4 ± 0.12
Ni–Co–P–0.5 g/L Fe_2O_3 annealed	0.58 ± 0.029	3.6 ± 0.216

3.8. Corrosion behaviour

The corrosion activity of the substrate with applying (Ni–P) and (Ni–P–Fe_2O_3) composite coating, respectively, has been examined in 3.5 % NaCl. Solutions. Potentiodynamic polarization is being used to provide predictions regarding the corrosion behavior of alloys. Table 5 shows the corrosion characteristics of corrosion current density (I_{corr}) and corrosion rate (*CR*) obtained from corrosion tests performed on specimens in 3.5 % NaCl. solution" at 371 °C. The following equation is used to calculate the rate of corrosion [24].

$$Corrosion\ rate\ = \frac{(0.13\ Icorr(Ew))}{\rho}, \quad (2)$$

where *Ew* is the equivalent weight (g/eq.); ρ is the density (g/cm^3); 0.13 is the metric and time conversion factor; I_{corr} is the corrosion current density ($\mu A/cm^2$).

Table 5. Corrosion current density (I_{corr}) and corrosion rate (CR) for all samples in 3.5 % NaCl solution at 37 ± 1 °C

Sample	E_{corr}, mV	I_{corr}, μA	Corrosion rate, mpy
Substrate	-571	49.4	7.11 ± 0.355
Ni–P annealed	-471	0.337	0.047 ± 0.002
Ni–P–0.1 g/L Fe_2O_3 annealed	-120	0.3	0.042 ± 0.0021
Ni–P–0.3 g/L Fe_2O_3 annealed	-157	1.2	0.168 ± 0.008
Ni–P–0.5 g/L Fe_2O_3 annealed	-501	24.3	3.417 ± 0.17

Potentiodynamic polarization curves were measured on uncoated and Ni–P and Ni–P–Fe_2O_3-coated 4140 steel, as shown in Fig. 10, indicating less harmful (E_{corr}) values for heat-treated specimens. It is clear that the Ni–P coating is used to enhance the properties of the AISI 4140 steel and the corrosion is due to the uniform thickness of electroless deposition and the ability of the Ni–P coating to be an effective barrier between corrosion media and metal. It should be noted that the value of E_{corr} is less harmful, and the rate of corrosion and Icorr is lower on the plated sample than on the uncoated sample [19]. However, the addition of Fe_2O_3 is very innovative. Samples are coated with different Fe_2O_3 concentrations and soaked in a solution of 3.5 % NaCl. Then, the curves of polarization are evaluated. Fig. 10 shows the effect of Fe_2O_3 on the curve of polarization.

Table 5 shows the potential of corrosion in different concentrations of Fe_2O_3. In the 0.1 g/L Fe_2O_3 concentration, the I_{corr} of the Ni–P–Fe_2O_3 composite coating is 0.3 μA, and the I_{corr} of the Ni–P coating is 0.337 μA; the addition of Fe_2O_3 makes the coating denser when compared with a coating of Ni–P, which means that resistance to the corrosion for the composite coating was better. When there is an increase in the Fe_2O_3 concentration to 0.5 g/L, a higher region of Fe_2O_3 agglomeration is noted; this is unfavorable to coating, as it reduces resistance to corrosion of the composite coating. Other researchers have confirmed this [10, 11, 20]. This also indicates that the results of the composite coatings protected the substrate from corrosion. These samples had a lower corrosion rate and higher microhardness [21 – 23]. Yazdani S. et al. [28] indicated that increasing the CNT concentration to 1 gr/lit enhances the agglomeration phenomenon, consequently leading to a non-uniform distribution of nickel atoms on the coating surface. The latter leads to localized corrosion in this sample. Furthermore, as was stated in the previous section, by increasing CNT concentration up to 1 gr/lit, the crystallization of the nickel atoms increases, and the structure of the coating changes from amorphous to semi-crystalline, this leads to a higher surface energy of the coating due to the accumulation of dislocations and leads to a higher corrosion rate.

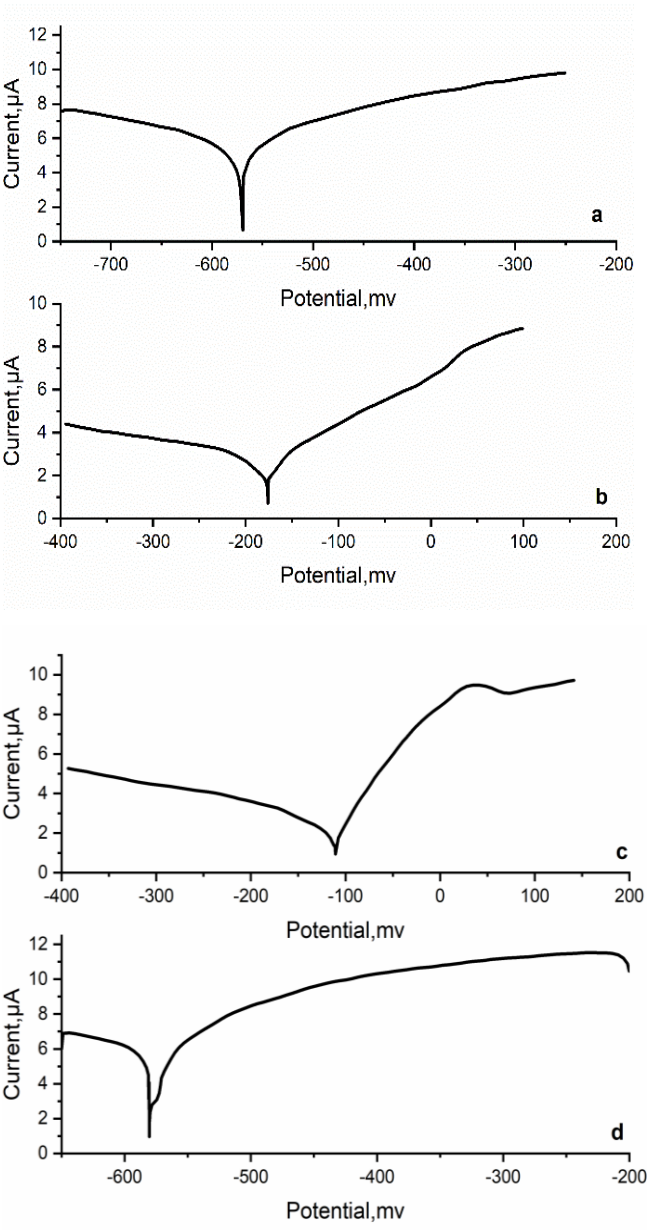

Fig. 10. Polarization of Tafel curves: a – as-substrate; b – Ni–P; c – Ni–P–0.1 g/l Fe_2O_3; d – Ni–P–0.3 g/l Fe_2O_3 annealed samples

4. CONCLUSIONS

The present work aimed to investigate the effect of Fe_2O_3 on wear behaviour and corrosion resistance of electroless Ni–P coating with different Fe_2O_3 concentrations on AISI 4140 steel coating. Optical images of the microstructure of carbon steel revealed pro eutectoid ferrite α plus pearlite phases. The pearlite consisted of ferrite interlaced with laths of cementite (Fe_3C). The ferrite grain shape was irregular, with a grain size of about 10 μm. The results show that the Fe_2O_3 particles were successfully embedded in the Ni–P and Ni–P–Fe_2O_3 composite coatings on the steel substrates with the electroless process. The better addition percentage of Fe_2O_3 to the Ni–P coating was 0.1 g/L. The microhardness and wear resistance of the Ni–P–Fe_2O_3 composite coatings turned out to be higher than the Ni-P coating. Both these improvements in the mechanical/tribological properties of the composite coating resulted from the presence of the dispersed particles of Fe_2O_3, which effectively hindered the grain dislocation during the microhardness and wear testing processes. An improvement ratio of 107 % for microhardness and 90% for reduction-specific wear rate. Ni–P and Ni–P–Fe_2O_3 composite coatings improved the corrosion resistance of the coated specimen. However, the effect was more pronounced in the case of Ni–P–Fe_2O_3 as compared to Ni-P coating, and the improvement ratio was 99.4 %, reducing the corrosion rate and decreasing the friction coefficient to 0.42 was achieved by the heat treatment of Ni–P–Fe_2O_3 (0.1 g/L Fe_2O_3) at 400 °C for 1 h.

REFERENCES

1. **Yanmei, L.I., Chiate, L.I.U., Liang, Y., Xiaotong, C.H. E.N., Zhibiao, Y.A.N.G., Yingjun, C.H.E.N.** The Long-term Corrosion Behaviors of SLM 316L Stainless Steel Immersed in Artificial Saliva *Materials Science (Medžiagotyra)* 28 (2) 2022: pp. 196 – 201. http://dx.doi.org/10.5755/j02.ms.28636
2. **Ayoub, I.** Study of Electroless Ni-P Plating on Stainless Steel *Isotope and Radiation Research* 41 (4s2) 2009: pp. 1551 – 1559.
3. **Petrova, M., Noncheva, Z., Dobreva, E.** Electroless Deposition of Nanocomposite Nip-Coatings on Metal Substrates *International Scientific Colloquium* 51 2006.
4. **Jiaqiang, G., Lei, L., Yating, W., Bin, S., Wenbin, H.** Electroless Ni–P–SiC Composite Coatings with Superfine Particles *Surface and Coatings Technology* 200 (20 – 21) 2006: pp. 5836 – 5842. https://doi.org/10.1016/j.surfcoat.2005.08.134
5. **Gadhari, P., Sahoo, P.** Study of Tribological Properties of Electroless Ni–P–Al_2O_3 Composite Coatings *IOSR Journal of Mechanical and Civil Engineering (IOSR-JMCE)* Special Issue 2014: pp. 34 – 34.
6. **Gadhari, P., Sahoo, P.** Improvement of Corrosion Resistance of Ni–P–Al_2O_3 Composite Coating by Optimizing Process Parameters Using Potentiodynamic Polarization Test *Portugaliae Electrochimica Acta* 32 (2) 2014: pp. 137 – 156. https://doi.org/10.4152/pea.201402137
7. **Ray, T.** Evaluation of Electroless Nickel-Phosphorus (EN) Coatings. PhD thesis, Department of Mechanical Engineering University of Saskatchewan, 2003.
8. **Zhao, H., Fu, W., Yang, H., Xu, Y., Zhao, W., Zhang, Y.** Synthesis and Characterization of TiO_2/Fe_2O_3 Core-shell Nano Composition Film and their Photo Electrochemical Property *Applied Surface Science* 257 (21) 2011: pp. 8778 – 8783. https://doi.org/10.1016/j.apsusc.2011.04.004
9. **Khalifa, O.R.M., Sakr, E.** Electroless Nickel-Phosphorus-Polymer Composite Coatings *The Open Corrosion Journal* 2 (1) 2009: pp. 211 – 215. https://doi.org/10.2174/1876503300902010211
10. **Haq, I.U., Akhtar, K., Khan, T.I., Shah, A.A.** Electrodeposition of Ni–Fe_2O_3 Nanocomposite Coating on Steel *Surface and Coatings Technology* 235 2013: pp. 691 – 698. https://doi.org/10.1016/j.surfcoat.2013.08.048
11. **Shibli, S., Sebeelamol, J.** Development of Fe_2O_3–TiO_2 Mixed Oxide Incorporated Ni–P Coating for Electrocatalytic

Hydrogen Evolution Reaction *International Journal of Hydrogen Energy* 38 (5) 2013: pp. 2271 – 82. https://doi.org/10.1016/j.ijhydene.2012.12.009

12. **Lenard, J.G. Primer on Flat Rolling.** Elsevier Linacre House, Jordan Hill, Oxford, UK, 2007: pp.186.
13. **Samuels, L.E.** Light Microscopy of Carbon Steels, ASM International, USA, 2003: pp. 361.
14. **Hou, K., Ger, M., Wang, L., Ke, S.** The Wear Behaviour of Electro-codeposited Ni–SiC Composites *Wear* 253 (9 – 10) 2002: pp. 994 – 1003. https://doi.org/10.1016/S0043-1648(02)00222-3
15. **Shi, L., Sun, C.F., Zhou, F., Liu, W.M.** Electrodeposited Nickel–cobalt Composite Coating Containing Nano-sized Si_3N_4 *Materials Science and Engineering: A* 397 (1 – 2) 2005: pp. 190 – 194. https://doi.org/10.1016/j.msea.2005.02.009
16. **Lajevardi, S., Shahrabi, T.** Effects of Pulse Electrodeposition Parameters on the Properties of Ni–TiO_2 Nanocomposite Coatings *Applied Surface Science* 256 (22) 2010: pp. 6775 – 6781. https://doi.org/10.1016/j.apsusc.2010.04.088
17. **Ma, L., Zhou, K.C., Li, Z.Y., Wei, Q.P.** Electrodeposition of Ni-Co-Fe_2O_3 Composite Coatings *Journal of Central South University of Technology* 17 (4) 2010: pp. 708 – 714. https://doi.org/10.1016/j.surfcoat.2013.08.048
18. **Yan, M., Ying, H., Ma, T.** Improved Microhardness and Wear Resistance of the As-deposited Electroless Ni–P Coating *Surface and Coatings Technology* 202 (24) 2008: pp. 5909 – 5913. https://doi.org/10.1016/j.surfcoat.2008.06.180
19. **Araghi, A., Paydar, M.H.** Electroless Deposition of Ni–P–B4C Composite Coating on AZ91D Magnesium Alloy and Investigation on its Wear and Corrosion Resistance *Materials & Design* 31 (6) 2010: pp. 3095 – 3099. https://doi.org/10.1016/j.matdes.2009.12.042
20. **Li, J., Sun, Y., Sun, X., Qiao, J.** Mechanical and Corrosion-Resistance Performance of Electrodeposited Titania–nickel Nanocomposite Coatings *Surface and Coatings Technology* 192 (2 – 3) 2005: pp. 331 – 335. https://doi.org/10.1016/j.surfcoat.2004.04.082
21. **Wai, A.M.H., Ali, A.R.K.A., Mahoub, F.** Comparing the Effect of Heat Treatment and Plasma-nitridingon Corrosion Resistance of Ni-B-CNT Electroless Coating with Different CNT Concentration on AISI 4340 Steel *International Journal of Mechanical and Production Engineering Research and Development* 9 (5) 2019: pp. 183 – 196.
22. **Abidali, A.R.K., Wais, A.M.H.** Study the Effects of Carbon Nano Tubes on Corrosion Behavior of Ni-pelectro-less Coating of Low Alloy Steels in Salt Water *International Journal of Mechanical and Production Engineering Research and Development* 9 (5) 2019: pp. 137 – 146.
23. **Muna, I., Karthik, K., Hemalatha, P., Shady, E., Omar, Sh., Mohammad, I., Ranin, Z., Kishor, K.** Enhanced Corrosion Protection of Epoxy/ZnO-NiO Nanocomposite Coatings on Steel *Coatings* 10 (8) 2020: pp.783. https://doi.org/10.3390/coatings10080783
24. **Kayalı, Y., Yönetken, A.** Investigation of Wear Behavior of Borided Materials Produced by the Powder Metallurgy Method in Different Compositions *Protection of Metals and Physical Chemistry of Surfaces* 57 (4) 2021: pp. 771 – 778. https://doi.org/10.1134/S2070205121040122
25. **Yönetken, A., Erol, A.** The Effect of Microwave Sintering on the Properties of Electroless Ni Plated WC-Fe-Ni Composites *Science and Engineering of Composite Materials* 17 (3) 2010: pp. 191 – 198. https://doi.org/10.1515/SECM.2010.17.3.191
26. **Yonetken, A., Talaş, Ş., Erol, A., Gökoğlan, Ö., Mersin, T.** Production and Wear Property of Electroless Ni-plated B4C-AstaloyCr-M Composites *Science and Engineering of Composite Materials* 22 (3) 2015: pp. 251 – 255. https://doi.org/10.1515/secm-2013-0061n
27. **Yönetken, A.** Fabrication of Electroless Ni Plated Fe–Al_2O_3 Ceramic–metal Matrix Composites *Transactions of the Indian Institute of Metals* 68 (5) 2015: pp. 675 – 681. https://doi.org/10.1007/s12666-014-0497-1
28. **Yazdani, S., Mahboubi, F., Tima, R., Sharifahmadian, O.** Effect of Carbon Nanotube Concentration on the Corrosion Behavior of Electroless Ni-B-CNT Coating *Journal of Materials Engineering and Performance* 28 (6) 2019: pp. 3446 – 3459. https://doi.org/10.1007/s11665-019-04155-3